Assessment of irradiated socket healing in the rabbit's mandible: Experimental study

Desoutter Aline, Barrot Laura, Langonnet Stephan, Béra Jean-Christophe, Chaux Anne-Gaëlle

Assessment of irradiated socket healing in the rabbit's mandible: experimental study

Aline Desoutter[1,2,3], Laura Barrot[2,3], Stephan Langonnet[3], Jean-Christophe Béra[2], Anne-Gaëlle Chaux[1,2,3,4].

1: Léon Bérard Cancer Center, Head and neck Unit, Surgery department, 28 rue Laennec 69008 Lyon, France

2: Labtau – Inserm 1032 Centre Léon Bérard, Université Lyon 1151 cours Albert Thomas 69008 Lyon

3: ICE (Experimental Surgery Institute) Léon Bérard Cancer Center, 28 rue Laennec 69008 Lyon, France

4: University Claude Bernard Lyon I, Lyon, France

Corresponding author:

Dr Anne-Gaëlle Chaux

Centre Léon Bérard

28 rue Laennec

69008 Lyon

Tel +33478782959

Fax:+33478782701

E-Mail:anne-gaelle.bodard@lyon.unicancer.fr

Conflict of Interest Statement

The authors declare that there is no conflict of interest.

Abstract:

As bone healing is altered after external radiation therapy, its evaluation is mandatory and lacks in clinical practice. The aim of the pilot study was to validate micro computed tomography (microCT) as a simple and reliable technique for assessing irradiated bone healing in the rabbit's mandible and compare with histologic findings.

Nineteen rabbits (female New Zealand white) were used. The radiation protocol consisted of 5 sessions delivering 8.5 Gy each. MicroCT was performed at D0, D7, D14, D28 and D42 for the control group and D0, D28 and D42 for the irradiated group. A modified Perry's score was determined on histologic samples, and comparison between microCT and histological findings was performed.

The main differences between irradiated and non-irradiated rabbits were observed at Day 28 and 42. There was a strong correlation between imaging and histologic findings.

Radiation decreases bone quality and bone mineral density. As the correlation was strong between microCT and histologic findings, micro imaging could be considered as a simple and reliable technique to assess bone healing after radiation therapy and allows an easy comparison between samples, without invasive procedures. Great attention should be kept on the parameters and on the region of interest.

The development of in-vivo microCT enlarges the perspectives of microCT use in experimental studies, avoiding invasive procedures, and preserving animal lives and well-being, and furthermore lead to clinical applications.

Key words

External radiotherapy

Bone healing

45 Microscanner (microCT)

46

47 **Introduction**

48 External radiotherapy is widely used in the treatment of head and neck squamous cell
49 carcinomas, with a mean 50 to 70 Gy total dose of irradiation. Its adverse effects on bone are
50 well described: it causes vascular alterations, cell decrease and an increase of collagen
51 excretion, leading to bone weakness and fibrosis. Thus, it compromises bone healing and can
52 lead to osteoradionecrosis (ORN) (Lyons and Ghazali, 2008; Jacobsson et al., 2010). ORN
53 mostly presents as an area of exposed, avascular bone, frequently infected. Its early stage is
54 characterized by inflammation and presence of myofibroblasts, and a decrease of bone
55 remodeling. ORN can occur spontaneously or after oral surgery. It is generally diagnosed
56 quite late as clinical symptoms are not consistent, and its radiological expression appears
57 when the necrosis is already set up, when 30 to 40% of the mineralized phase is altered. The
58 treatment of ORN depends on its stage: early stages require medical treatment associated with
59 bone curettage, whereas advanced stages can lead to interruptive surgery followed by
60 reconstructive surgery (using free bone flaps when possible). There is currently no tool in
61 clinical routine for assessing bone quality ; orthopantomographs are not performant enough,
62 and computed tomography (CT scan) shouldn't be performed too often. In experimental
63 studies, microimaging and histology are the gold standard in bone evaluation (Donnelly,
64 2011). Histology is often used as a reference to assess bone healing. In clinical practice, as
65 histology is invasive and can itself lead to ORN, it cannot be performed ; standard CT scan
66 are quite irradiating and must also be used sparingly. Thus, there is a need of easy-to-use and
67 non-destructive tools for the follow up of irradiated bone. Through the development of an
68 animal model of irradiated mandible, the aim of the study was to compare microscanner
69 (microCT) imaging and histological findings in the follow up of irradiated bone healing.

Material and methods

Animals

The protocol was conducted in accordance with international and local laws, guidelines and policies on animal welfare. It was approved by the internal ethics committee for animal experimentation of the Research Institute in which it was performed (CEEA n°10). The research protocol followed the ARRIVE guidelines.

Nineteen New Zealand adult female rabbits were used (weight: mean: 2.35 kg ; SD: 0.53). Animals were randomly divided into 2 groups, one control group on which only surgery was performed; and one experimental group with radiotherapy and surgery (table 1). It resulted in 10 samples for the control group and 9 samples for the irradiated group, which led to respectively 300 and 270 histologic sections, and 150 and 135 images.

Radiation therapy

External radiotherapy was performed on a 6MeV photons linear accelerator and consisted of 5 weekly sessions delivering 8.5 Gy each, on a linear accelerator delivering 6MeV photons, as described in a previous publication (Desoutter et al., 2020), with an alpha/beta ratio of 2. The animals were sedated with intramuscular administration of ketamin / xylazin / glycopyrolate 15 minutes before the session. A catheter was then placed in the vein of the ear to allow control of sedation by periodical re-injection. A scanner had been previously performed to calculate the dosimetry. The rabbits were transported to the radiation room according to the protocol of the Research Institute, and immediately installed on the accelerator. The sedation was controlled immediately before the beginning of irradiation. A thermoformed mattress was used to enhance the precision of the repositioning, and a silicon sheet was placed to increase the thickness of the soft tissues and concentrate the maximal dose on bone. Before the beginning of the irradiation, a radiograph was performed to validate the radiation field and

control the positioning of the animal. At the end of the session, the animals were placed under infrared light and monitored until complete recovering. The follow up was performed by daily examination, weighting and control of food and water intake. Standard limit points, defined by the ethics committee, were: fever, permanent decubitus, convulsions, severe anemia, pain symptoms resistant to analgesia procedures and anorexia superior to 24 hours.

The total dose delivered was 42.5 Gy which is equivalent to 98 Gy in human. Animals were sacrificed at D0, D7, D14, D28 and D42 in the control group and D0, D28 and D42 in the irradiated group.

Surgery

A standardized defect (2x3 mm) at 5 mm mesially to the mental foramen on each side of the mandible was performed immediately after completion of radiotherapy, by an extraoral surgical approach. Sedation was performed as previously described; analgesics (ketoprofen) were administered immediately and if necessary during the follow up. Euthanasia was performed after sedation thanks to intravenous 4ml pentobarbital. Samples were harvested thanks to the same submental approach. They were immediately placed into ethanol and sent to the microCT. Then, the samples were immediately sent for histologic analysis. Each sample was analyzed by microCT and then by histology.

Microscanner

Rabbits were sacrificed from D0 (i.e. the day of the surgery) to D42 by 4 ml intravenous pentobarbital. MicroCT analyses were performed by 2 experimented operators.

The microCT (Inveon®, Siemens) was performed according to standards for bone characterization in the rodent (Faot et al., 2015; Müller, 2009) with high magnification, 180 projections; binning 2, pixel size: 18.76microm ; axial and transaxial fields of view were respectively 18 mm and 28.16mm, scanning length 18 mm. Voltage was 75 kV, and current

500 microA. Exposure time was 770ms and acquisition 36 minutes. A Hounsfield and density calibration was daily performed. The volume of interest (VOI) was determined thanks to points of reference calculated from the top of the defect. As the defect was standardized, remarkable points were identified to allow comparison between the different samples: top of the defect (bone crest), and apex of the defect. Microradiographic slices were performed every 5 slices, resulting in 30 images per sample for analysis. BV/TV (percent bone volume), TbN (trabecular number) and TbSp (trabecular separation) were reported and analyzed thanks to ImageJ® (NIH) software. The bone mineral density (BMD) was also determined using microCT values (Hounsfield units).

Histology

Samples were fixed in 10% formalin, embedded in paraffin after slow decalcification in 0.5M EDTA for 1 month, sliced (30 slices per sample ; thickness : 8 micrometers) and stained with hematoxylin-eosin. A modified Perry's score (Perry et al., 2003) was used to assess bone healing and assigned by 2 independent operators (table 2). Operators were blinded and did not know if the samples were from the control or irradiated group, and which time interval was concerned.

Statistics

Statistical analysis was performed thanks to SPSS (SSPS.inc, IBM, Chicago, IL, USA). Standard deviation was calculated, and a T test was performed to compare the groups in terms of BMD, BV/TV, TbSp and TbN. Pearson's correlation coefficient was used to allow the comparison between histologic findings and microCT: Perry's score and BMD, Perry's score and BV/TV, Perry's score and TbN, Perry's score and TbSp.

Results

142 Experiments resulted in 10 samples for the control group and 9 samples for the irradiated
143 group, which resulted in respectively 300 and 270 histologic sections, and 150 and 135
144 images for Perry's score determination. Weight increased in both groups during the
145 experiment (mean: 121% ; SD : 56 in the non-irradiated group and 105% ; SD : 49 in the
146 irradiated group). Adverse effects observed were mild fugitive anorexia, light cough and very
147 localized alopecia.

148 Visual examination

149 The defect was visible only at D0 for the control group, and visible at any time in the
150 irradiated group. For the irradiated samples, the bone appeared less mineralized and weaker
151 during harvesting, with less resistance to the saw.

152 MicroCT

153 The defect was visible at D0 in the control group, and non-visible at D28 and D42. In the
154 irradiated group, the defect was visible at any time (figure 1).

155 The values at D0, D28 and D42 for BV/TV, TbSp, BMD and TbN are presented in table 3. In
156 the control group, the increase of BV/TV and TbN values was more significant between D0
157 and D28, whereas it was between D28 and D42 in the irradiated group. The difference
158 between the 2 groups was statistically significant at D28 and D42, except for TbSp, which
159 was the same in the control group between D28 and D42 (table 3).

160 Histology

161 For the control group, at D28 and D42, the defect was completely filled by mature bone.

162 In the irradiated group, the defect was not completely filled, even for D42. Only fibrovascular
163 tissue could be found, with only little area of bone in the defect. Necrotic tissue with areas of
164 adipous cells was reported, but no areas of osteoradionecrosis were noticed.

Modified Perry's scores were respectively at D0, D28 and D42: 1, 7 and 9 for control group, and 1, 2 and 3 for irradiated group (figure 2).

Pearson's correlation coefficients found strong positive correlation between modified Perry's scores and BMD, TbN and BV/TV, and strong negative correlation between Perry's score and TbSp (table 4).

Discussion

Rabbits are considered as a valuable model for initial experimentation evaluation, despite major differences with humans. The bone turnover is highly increased, and the bone marrow is fatty (Poort et al., 2014; Poort et al., 2017; Ma and Chen, 2012).

Animals

Among usual radio-induced adverse effects, only alopecia, cough and mild anorexia were reported, in a very mild expression, as described by Zhang (Zhang et al., 2010). It corroborates the high healing potential in the rabbit, and thus the need of higher doses to reproduce adverse effects similar to humans.

Radiation therapy

Several protocols were reported for experimental external radiotherapy (Perry et al., 2003; Soares et al., 2019; Poort et al., 2017). The protocol used in this study has already been described (Desoutter et al., 2020). Fractionated irradiation was preferred to single-dose as it better mimics human therapeutic irradiation (Zong et al., 2016). A dose of 8.5 Gy per session was proposed, and mandatory to observe adverse effects on bone, according to Zhang (Zhang et al., 2010).

MicroCT

MicroCT has a great interest in the analysis of bone structure (Donnelly, 2011; Müller, 2009) as it allows the assessment of 3D bone geometry, BV/TV, trabecular thickness, number and separation. Apparent BMD can also be calculated using the Hounsfield unit scale. The parameters chosen for microCT analysis (BV/TV, TbN, TbSp and BMD) are concordant with the literature (Donnelly, 2011; Müller, 2009). The problem was the identification of the VOI particularly in the control group as bone healing seemed to be almost completed at D28. Moreover, there might be a difficulty to choose the threshold parameters to separate bone trabeculae and marrow space, which may influence the images. In irradiated bone, it seems that bone density is correlated to the radiation dose, the time interval between radiotherapy and examination, and the use of hyperbaric oxygen therapy (HBO) (Zong et al., 2016; Muhonen et al., 2002). Comparing the control and the irradiated groups, BV/TV was divided by a factor of 33.81 at D28, and 5.34 at D42. BMD was divided by 1.41 at D28 and 1.5 at D42; and TbN by 12.28 at D28 and 2 at D42. The fact that BV/TV and TbN dramatically increase between D0 and D28 in the control group and between D28 and D42 in the irradiated group is concordant with the fact that it takes more time to heal in irradiated bone. In the irradiated group, TbSp decreased between D28 and D42 because complete bone healing was not reached.

MicroCT represents a valuable tool for the evaluation of radio-induced alterations, as a decrease of bone remodeling and a delayed healing are early signs of osteoradionecrosis. At this early stage, its treatment is less invasive and its recovery with only little sequelae remains possible.

Histology

Hematoxylin/eosin staining was used, as it is a routine, quick and easy-to-use staining, and is often reported in experimental studies on bone (Poort et al., 2014). Perry (Perry et al., 2003) described his score to rapidly assess bone and cartilage healing. It is a subjective score, based

on observation and the maturation of bone and cartilage. The modified Perry's score evaluates only bone as it is used in the mandibular corpus. It distinguishes different stages of bone maturation: fibrous tissue, non-mineralized bone (i.e there are some bone cells and part of components of bone, but no or little mineralized tissue), woven bone (i.e. immature mineralization, and/or anarchic mineralization), and mature bone. Perry's scores (figure 2) suggest that irradiated bone healing is delayed as the scores at each examination time interval were significantly lower in the irradiated group. It also suggests a more linear kinetics of bone healing in irradiated bone than in non-irradiated bone, but it must be proven by further investigations. Nonetheless, it is a subjective analysis, and potentially controversial.

Reliability of the use of microCT for assessing bone healing

MicroCT has been widely used in assessing bone healing, even in jaw bones (Faot et al., 2015; Clark and Badea, 2014; Van Dessel et al., 2013). Its use allows assessment of bone structure, resorption, remodeling, healing and destruction in several species (Hutchinson et al, 2017). Variables generally used are BMD, TbN, TbSp, BV/TV (Faot et al., 2015; Van Dessel et al., 2013; Hassumi et al., 2018; Mabileau et al., 2015; Parsa et al., 2013). Trabecular thickness can also be assessed (Van Dessel et al., 2013; Hassumi et al., 2018; Iezza et al., 2020). MicroCT has a high spatial resolution, and a high contrast is possible in imaging mineralized tissues (Clark and Badea, 2014), even for cartilage (De Bournonville et al., 2019). New tools such as 3D reconstruction, contrast enhancement or methods of overimposing images increase its effectiveness (Piotrowski at al., 2018; Hassumi et al., 2018; Mabileau et al., 2015). 3D reconstruction tools such as maximum intensity projections (MIP) can also be used (Piotrowski et al., 2018). Most of the authors report that micro CT allows precise assessment of bone microarchitecture, direct measurements of different parameters, analyses a larger region of interest than 2D histology, is fast and non-destructive, which is interesting both in living animals and in experimental studies (Faot et al., 2015; Müller, 2009; Van

238 Dessel et al., 2013; Parsa et al., 2013; Bouxsein et al., 2010; Kim and Henkin, 2015).
239 Nonetheless, to guarantee a good reliability, several steps must be respected. The sample
240 preparation and positioning is essential (Bouxsein et al., 2010). A special care must be given
241 to the determination of the region of interest (ROI): a starting point must be determined to
242 make comparable and reproducible acquisitions. The method used is generally not or
243 insufficiently described in the literature (Faot et al., 2015); the number of slices can help
244 giving points of reference, starting from a remarkable starting point (Hassumi et al., 2018), or
245 a marker can be used (Kim and Henkin, 2015). The segmentation must be standardized, and
246 thresholds must be adjusted based on empirical evaluation of attenuation properties, prior to
247 image acquisition (Poundarik and Vashishth, 2015). Thus, it is important to perform images to
248 compare on the same machine. Intensity, beam hardering and X-ray energy have to be
249 carefully chosen, as well as voxel size and image resolution. Image analysis should take
250 artifacts into account (Bouxsein et al., 2010). Using the Hounsfield Units scale is
251 controversial: for Pauwels (Pauwels et al., 2015), analyses based on quantitative grey values
252 are not reliable, whereas there is a high correlation score (0.91) between HU scale and BV/TV
253 for Parsa (Parsa et al., 2013).

254 Comparison between microCT and histology

255 Most of the studies used both microCT and histology or histomorphometry. Some assessed
256 the comparability between these 2 techniques (Bissinger et al., 2017; Boca et al., 2017; Choi
257 et al., 2019). MicroCT was more accurate for evaluating bone-implant contact as it was
258 nondestructive and provided a 3D picture of the ROI (26-28). Moreover, Particelli (Choi et
259 al., 2019) reported that there was a good correspondence between histological findings and
260 microCT, and that microCT had the advantage to not being affected by the surrounding
261 medium (for example the embedding material) when the threshold was accurately chosen. In
262 this study, microCT was compared to a histologic score. Piotrowski (Piotrowski et al., 2018)

proposed to use a score based on MIP reconstruction to assess bone healing. Histologic analysis was also performed and seemed to be in accordance with microCT findings.

Our findings suggest that micro CT accurately reflects histologic findings, with very strong correlation coefficients.

Limitations of the study

The major bias of the study (apart from the number of samples which could be discussed) was the use of the modified Perry's score, which remains subjective despite double scoring, and does not reflect the continuous process of bone healing.

Conclusions

The radiation scheme used in this study seemed to decrease bone healing, both histologically and radiologically. Despite unavoidable bias, this study seemed to confirm the correlation between microCT and histological findings in irradiated bone healing. MicroCT seems to be a valuable non-invasive tool for evaluating early stages of radio-induced bone alterations, which is particularly interesting as even a small trauma (i.e; bone harvesting for histologic analysis) can lead to osteonecrosis. The development of micro CT in-vivo procedures and 3-dimensional reconstruction tools (Pauwels et al., 2015; Boca et al., 2017; Choi et al., 2019) will allow nondestructive methods for basic evaluation of mineralized tissues and will reserve histology, which is destructive and often requires animal sacrifice, to specific markers or techniques.

Funding:

This work was supported by the Institut Français pour la Recherche Odontologique (2012 and 2019)

And the Focused UltraSound Foundation (2018)

Figure legends

Table 1: number of samples per group (control and irradiated) and per time interval for analysis

Table 2: Perry's modified score and its histological signification

Table 3: values for BV/TV, BMD, TbN, TbSp for each group and p values (i.e. statistical significance) between the groups

Table 4: Pearson's correlation coefficient for Perry's modified score and the different microCT parameters (BMD, BV/TV, TbN, TBSp).

Figure 1: representative microCT and histology samples of control and irradiated group at D0, D28 and D42.

Figure 2: Graph of the evolution of the modified Perry's score between D0 and D42 for control and irradiated groups.

References

Bissinger O, Probst FA, Wolff KD, Jeschke A, Weitz J, Deppe H, Kolk A. Comparative 3D micro-CT and 2D histomorphometry analysis of dental implant osseointegration in the maxilla of minipigs. J Clin Periodontol. 2017 Apr;44(4):418-427. doi: 10.1111/jcpe.12693. Epub 2017 Feb 27.

306 Boca C, Truyen B, Henin L, Schulte AG, Stachniss V, De Clerk N, Cornelis J, Bottenberg P.
307 Comparison of micro-CT imaging and histology for approximal caries detection. Scientif Rep
308 2017;7:6680.

309 Bouxsein ML, Boyd SK, Christiansen BA, Guldberg RE, Jepsen KJ, Müller R. Guidelines for
310 assessment of bone microstructure in rodents using micro-computed tomography. J Bone Min
311 Res 2010;25(7):1468-86.

312 Clark P, Badea CT. Micro-CT of rodents: state-of-the-art and future perspectives. Phys Med
313 2014;30(6):619-634.

314 Choi JY, Park JI, Chae JS, Yeo IL. Comparison of micro-computed tomography and
315 histomorphometry in the measurement of bone-implant contact ratios. Oral Surg Oral Med
316 Oral Pathol Oral Radiol. 2019 Jul;128(1):87-95. doi: 10.1016/j.oooo.2018.12.023. Epub 2019
317 Jan 4.

318 Desoutter A, Langonnet S, Deneuve S, Bera JC, Chaux AG. Validation of a rabbit model of
319 irradiated bone healing: preliminary report. JOMOS 2020 [accepted for publication]

320 De Bournonville S, Vangrunderbeeck S, Kerckhofs G. Contrast-enhanced micro-CT for
321 virtual 3D anatomical pathology of biological tissues: a literature review. Contrast Media and
322 Molecular Imaging 2019;8617406.

323 Donnelly E. Methods for assessing bone quality. Clin Orthop Relat Res 2011;469:2128-38.

324 Faot F, Chatterjee M, de Camargos GV, Duyck J, Vandamme K. Micro-CT analysis of the
325 rodent jaw bone micro-architecture: a systematic review. Bone Rep 2015;2:14-24.

326 Hassumi JS, Mulinari-Santos G, Fabris ALdS, Jacob RGM, Goncalves A, Rossi AC, Freire
327 AR, Faverani LP, Okamoto R. Alveolar bone healing in rats: microCT, immunohistochemical
328 and molecular analysis. J Appl Oral Sci 2018;26:e20170326

329 Hutchinson JC, Shelmerdine SC, Simcock IC, Sebire NJ, Arthurs OW. Early clinical
330 applications for imaging at microscopic detail: microfocus computed tomography (micro-CT).
331 Br J Radiol 2017;90:20170113

332 Iezzi G, Mangano C, Barone A, Tirone F, Baggi L, Tromba G, Piatelli A, Giuliani A.
333 Jawbone remodeling: a conceptual study based on synchrotron high-resolution tomography.
334 Scientif Rep 2020;10:3777

335 Jacobsson AS, Buchbinder D, Hu K, et al. Paradigm shifts in the management of
336 osteoradionecrosis of the mandible. Oral Oncol 2010; 46: 795-801.

337 Kim YJ, Henkin J. Micro computed tomography assessment of human alveolar bone: bone
338 density and three-dimensional microarchitecture. Clin Impl Dent Relat Res 2015;17(2):307-
339 13.

340 Lyons A, Ghazali N. Osteoradionecrosis of the jaws: current understanding of its
341 pathophysiology and treatment. Br J Oral Maxillofac Surg 2008; 46: 653-660.

342 Ma Y, Shen G. Distraction osteogenesis after irradiation in rabbit mandibles. Br J Oral
343 Maxillofac Surg 2012 ;50 :662-7.

344 Mabilleau G, Mieczkowska A, Libouban H, Simon Y, Audran M, Chappard D. Comparison
345 between X-ray imaging, dual energy X-ray absorptiometry and microCT in the assessment of
346 bone mineral density in disuse-induced bone loss. J Musculoskelet Neuronal Interact
347 2015;15(1):42-52.

348 Muhonen A, Peltomaki T, Hinkka S, Happonen RP. Effect of mandibular distraction
349 osteogenesis on temporomandibular joint after previous irradiation and hyperbaric
350 oxygenation. Int J Oral Maxillofac Surg 2002; 31(4): 397-404.

351 Müller R. Hierarchical microimaging of bone structure and function. Nat Rev Rheumatol
352 2009;5:373-81.

353 Parsa A, Ibrahim N, Hassan B, van der Stelt P, Wismeijer D. Bone quality evaluation at dental
354 implant site using multislice CT, microCT and cone beam CT. Clin Oral Impl Res 2013;0:1-7

355 Particelli F, Mecozzi L, Beraudi A, Montesi M, Baruffaldi F, Viceconti M. A comparison
356 between micro-CT and histology for the evaluation of cortical bone: effect of
357 polymethylmethacrylate embedding on structural parameters. J Microsc. 2012
358 Mar;245(3):302-10. doi: 10.1111/j.1365-2818.2011.03573.x. Epub 2011 Nov 22.

359 Pauwels R, Jacobs R, Singer RS, Mupparapu M. CBCT-based bone quality assessment : are
360 Hounsfield unites applicable. Dentomaxillofac Radiol 2015;44:20140238

361 Perry AC, Prpa B, Rouse MS, Piper KE, Hanssen AD, Steckelberg JM, Patel R. Levofloxacin
362 and trovafloxacin inhibition of experimental fracture healing. Clin Orthop Relat Res
363 2003,414:95-100.

364 Piotrowski SL, Wilson L, Dharmaraj N, Hamze A, Clark A, Tailor R, Hill LR, Lai S, Kasper
365 K, Young S. Development and characterization of a rabbit model of compromised
366 maxillofacial wound healing. Tissue Eng:part C 2019;25(3):160-167.

367 Poort L, Lethaus B, Böckmann R, Buurman D, De Jong J, Hoebers F, Kessler P.
368 Experimental studies on the irradiation of facial bones in animals: a review. Int J Oral
369 Otolaryngol Head Neck Surg 2014;3:113-27.

370 Poort LJ, Ludjage JHB, Lie N, Böckmann RA, Odekerken JCE, Hoebers FJ, Kessler PAWH.
371 The histological and histomorphometric changes in the mandible after radiotherapy: an animal
372 model. J Craniomaxillofac Surg 2017;45(5):716-21.

373 Poundarik A, Vashishth D. Multiscale imaging of bone microdamage. Connect Tissue Res
374 2015;56(2):87-98.

375 Soares PBF, Soares CJ, Limirio PHJO, Limirio PHJO, Rezende de Jesus RN, Dechichi P,
376 Spin-Neto R, Zanetta-Barbosa D. Effect of ionizing radiation after-therapy interval on bone:
377 histomorphometric and biomechanical characteristics. Clin Oral Invest 2019;23:2785-2793.

378 Van Dessel J, Huang Y, Depypere M, Rubira-Bullen I, Maes F, Jacobs R. A comparative
379 evaluation of cone beam CT and micro-CT on trabecular bone structures in the human
380 mandible. Dentomaxillofac Radiol 2013;42:20130145

381 Van Deweghe S, Coelho PG, Vanhove C, Wennerberg A, Jimbo R. Utilizing micro-computed
382 tomography to evaluate bone structure surrounding dental implants: a comparison with
383 histomorphometry. J Biomed Mater Res B Appl Biomater. 2013 Oct;101(7):1259-66. doi:
384 10.1002/jbm.b.32938. Epub 2013 May 10.

385 Zhang WB, Zheng LW, Chua D, Cheung LK. Bone regeneration after radiotherapy in an
386 animal model. J Oral Maxillofac Surg 2010;68:2802-9.

387 Zong C, Cai B, Wen X, Alam S, Chen Y, Guo Y, Liu Y, Tian L. The role of myofibroblasts in
388 the development of osteoradionecrosis in a newly established rabbit model. J Cranio
389 Maxillofac Surg 2016; 44: 725-733.

	Control group		Irradiated group	
Time interval	Histology	MicroCT	Histology	MicroCT
D0	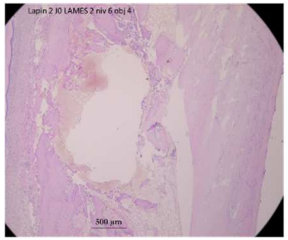	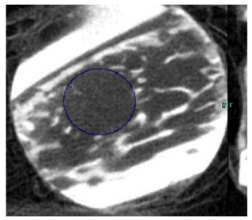	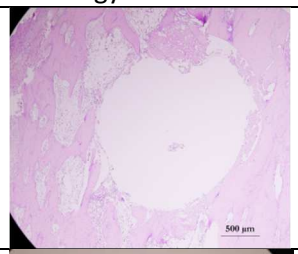	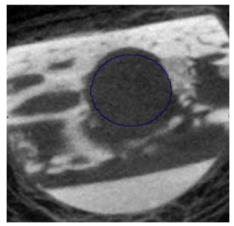
D28	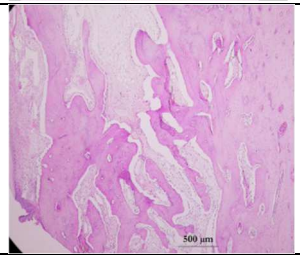	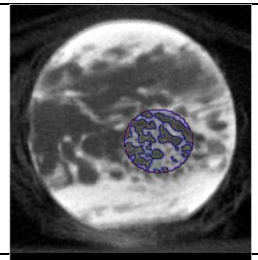	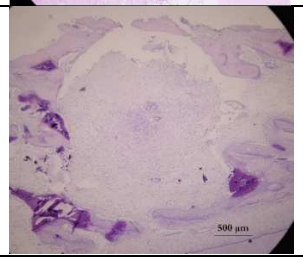	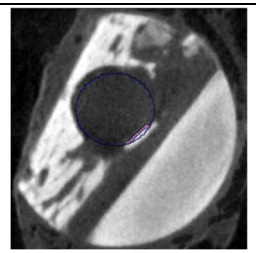
D42	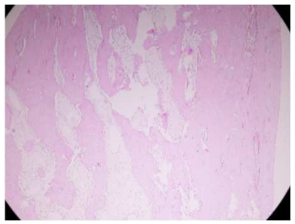	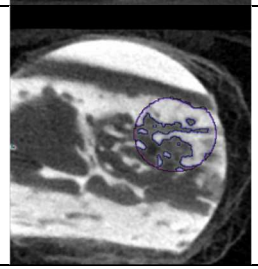	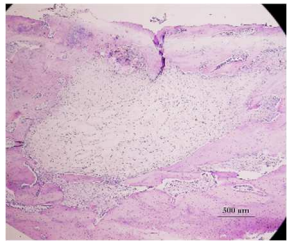	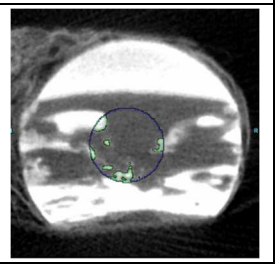

Histology (scale : 500 microm): In the control group: at D0, the defect is partially filled with blood; at D28, immature bone fills the defect; at D42, mature bone totally fills the defect. In the irradiated group: at D0, small amounts of blood are present, with less osteoblasts than the control group ; at D28: fibrous tissue is visible, no osteoclasts are visible ; at D42: osteoclasts are present, there is fibrous tissue and small amounts of immature bone.

Micro CT: Delineation of mineralized tissue was performed with Image J® software (NIH) ; the differences between the 2 groups are visible at each examination time interval.

Figure 3

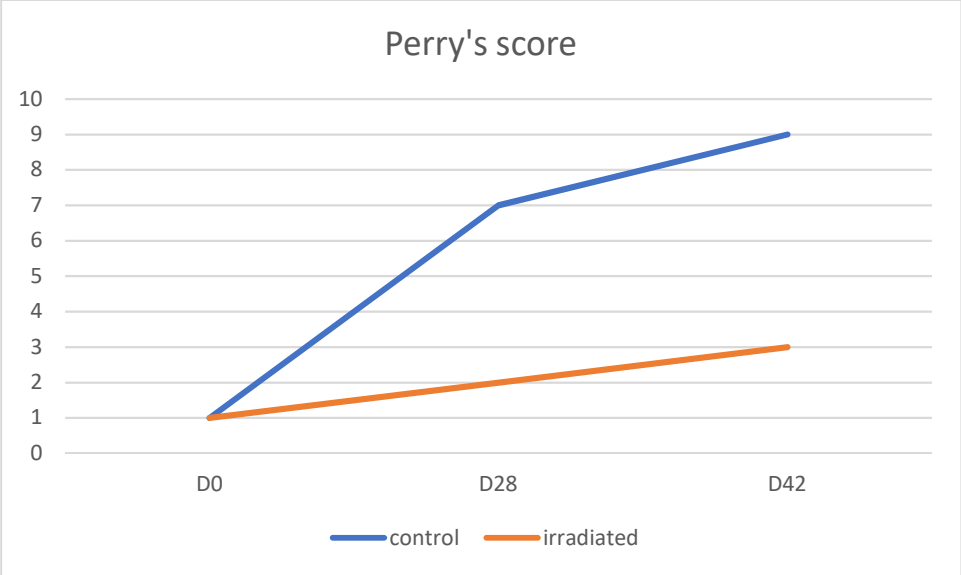

Table 1

Time for sacrifice (D : day)	Sham rabbits (number)	Irradiated rabbits (number)
D0	2	2
D7	2	0
D14	2	0
D28	2	4
D42	2	3

Perry's score	Histological observation (Perry's definition)	Modified Perry's observation
1	Fibrous tissue	Fibrous tissue
2	Mostly fibrous tissue and cartilage	Mostly fibrous tissue and some non-mineralized bone
3	Same amount of fibrous tissue and cartilage	Same amount of fibrous tissue and non-mineralized bone
4	Cartilage only	Non mineralized bone only
5	Predominant cartilage and a few woven bone	Predominant non-mineralized bone and a few woven bone
6	Equal amount of cartilage and woven bone	Equal amount of non-mineralized bone and woven bone
7	Predominant woven bone with a few cartilage	Predominant woven bone with a few non-mineralized bone
8	Woven bone only	Woven bone only
9	Woven bone and some mature bone	Woven bone and some mature bone
10	Mature bone	Mature bone

Table 3: Values for BMD, BV/TV, TbSp, TbN and Standard Deviation at D0, D28 and D42.

		Sham group		Irradiated group		P value
		Value (mean)	SD	Value (mean)	SD	
BMD	D0	1050.1	27.8	1038.8	131.2	NS
	D28	1620.1	74.6	1144.7	22.0	0.03
	D42	1677.2	9,60	1228.6	66,4	0.03
BV/TV	D0	1.48	0.6	0.22	0.2	NS
	D28	30.77	2.6	0.91	0.6	0.008
	D42	42.57	12,25	7.97	4,85	0.02
TbN	D0	0.14	0.05	0.02	0.01	NS
	D28	0.86	0.09	0.07	0.05	0.01
	D42	1.03	0,15	0.47	0.35	0.03
TbSp	D0	1.33	0.21	1.68	0.01	NS
	D28	0.38	0.08	1.35	0.26	0.01
	D42	0.36	0,06	0.92	0.30	0.04

NS: non statistically significant (p value ≥ 0.05).

Variable / Perry's score	Group	Value	Significance
BMD	Control group	0.999	Strong positive correlation
	Irradiated group	0.977	Strong positive correlation
BV/TV	Control group	0.985	Strong positive correlation
	Irradiated group	0.742	Strong positive correlation
TbN	Control group	0.997	Strong positive correlation
	Irradiated group	0.712	Strong positive correlation
TbSp	Control group	-0.951	Strong negative correlation
	Irradiated group	-0.954	Strong negative correlation